Understanding the nano-photonics absorption limit in both front-side and front/rear-side textured slabs

Ahmadpanahi, Hamed; Vismara, Robin; Isabella, Olindo; Zeman, Miro

DOI
10.1364/OE.27.0A1173

Publication date
2019

Document Version
Final published version

Published in
Optics Express

Research Article | Vol. 27, No. 16 | 5 Aug 2019 | OPTICS EXPRESS A1173
Optics EXPRESS

Understanding the nano-photonics absorption limit in both front-side and front/rear-side textured slabs

HAMED AHMADPANAHI,* ROBIN VISMARA, OLINDO ISABELLA AND MIRO ZEMAN

Department of Electrical Sustainable Energy, Delft University of Technology, Delft, Netherlands
**S.H.Ahmadpanahi@tudelft.nl*

Abstract: Surface texturing is one of the main techniques to enhance light absorption in solar cells. In thin film devices, periodic texturing can be used to excite the guided resonances supported by the structure. Therefore, total absorption is enhanced largely due to the excitation of these resonances. Although the maximum absorption enhancement limit in both bulk and photonic structures is known already, the weight of each resonance type in this limit is not yet clear. In this contribution, we extend the temporal couple-mode theory, deriving a closed formula to distinguish the contribution of Fabry-Perot and wave-guided modes within the absorption limit for 1-D grating structures. Secondly, using this analytical approach, we can clearly address cases of bulk and thin absorber thicknesses. Our results, supported by rigorous electromagnetic calculation, show that absorption enhancement in a 1-D grating structure can be much higher than the nano-photonic limit ($2\pi n$) reported by Yu et al. Thirdly, beyond the framework put forward by Yu et al., we extended our theory to describe the absorption enhancement in double side textured slabs. We have found that when the periods of top and bottom gratings are aliquant, absorption is enhanced in a wider frequency range. We provide rigorous numerical calculations to support our theoretical approach.

1. Introduction

The performance of solar cells is strongly linked to their light absorption capabilities [1]. Therefore, a significant amount of research has been dedicated to different light management techniques, in order to improve light absorption in the device active layer [2,3]. Light management is mostly focused on (i) the effective use of solar spectrum [4–10], (ii) maximizing the number of photons reaching the absorber layer [11–14], (iii) keeping the solar radiation energy inside the absorber long enough, until it is absorbed by the material. The first aspect can be achieved by employing spectrum splitters and multi-junction devices [15–18]. The second aspect is accomplished by applying anti-reflection coatings and by minimizing light absorption in non-active layers [19–24]. The third aspect, usually referred to as light trapping or optical path enhancement, is attained by altering the propagation direction of light such that total internal reflection inside the absorber occurs [25]. This is possible only if one or both surfaces of the absorber are textured. After hitting an interface with random texturing, incident light is scattered into propagation directions with a wide angular range [26–28]. The greater the scattering angle, the larger the optical path length enhancement. Optical path length enhancement is defined as l/d, with d representing the absorber physical thickness and $l = d/\cos\theta$, where θ is the scattering angle [29]. In 1982, Yablonovitch elaborated that in a weakly absorbing slab with a 2-D Lambertian scattering interface, an optical path length enhancement of $4n^2$ can be achieved (where n is the refractive index of the absorber material) [30]. The angular intensity distribution (AID) of a Lambertian scatterer obeys Lambert's cosine law [31] and has an isotropic angular response, independently of the light incident

#368571 https://doi.org/10.1364/OE.27.0A1173
Journal © 2019 Received 27 May 2019; revised 30 Jun 2019; accepted 11 Jul 2019; published 16 Jul 2019

angle. In defining the $4n^2$ limit, the material absorption is considered to be very small, because the angular intensity distribution (AID) follows Lambert's cosine law only if the slab is transparent (weakly absorbing). Furthermore, the thickness of slab is considered to be much larger than the incidence wavelength, and thus the light path can be defined in the framework of geometric optics. The $4n^2$ limit which is based on statistical ray optics, is nowadays commonly referred to as the Yablonovitch limit or Lambertian limit. The Lambertian limit holds for any angle of incidence from $-\pi/2$ to $+\pi/2$ (acceptance angle π) with zero being the normal and $\pm\pi/2$ grazing to the slab surface. By decreasing the acceptance angle of the cell from π to 2β, it is possible to increase the optical path enhancement from $4n^2$ to $4n^2/\sin 2\beta$ [32,33]. The limit of $4n^2/\sin 2\beta$, commonly employed in concentrator photovoltaic, is valid for bulk structures and can easily be calculated using geometrical optics. On the other hand, when the texturing size or the absorber layer thickness is comparable to the wavelength, wave effects of light become prominent [34]. Thus, some of the basic assumptions leading to conventional limit are no longer applicable. In 2010, Yu et al. showed that – in the wave optics regime – the light absorption enhancement factor can go far beyond the conventional Lambertian limit, using wavelength-scale grating structures [35,36]. This absorption enhancement (F), which is called the nano-photonic limit, was derived using statistical temporal coupled-mode theory and can be calculated using:

$$F = \frac{2\pi\gamma_i}{\alpha d\Delta\omega}\frac{M}{N} \tag{1}$$

where M and N are the total number of resonances and reflection (leaking) orders supported by the structure in the frequency range Δω, respectively; d is the absorber thickness; γ_i is the decay rate and it is linked to the material absorption coefficient α via $\gamma_i = \alpha c/n$, where c is the speed of light in vacuo and *n* is the real part of material refractive index. At each frequency range, M and N are strongly dependent on grating symmetry, arrangement of unit cell and thickness of the absorber. At each frequency, a grating waveguide supports many modes. Each mode at each frequency in the waveguide propagates in different angle (different propagation angle). On the other hand, the grating scatters the incidence energy into many different angles (diffraction angles). If, at one particular frequency, a diffraction angle is equal to the propagation angle of a mode, then that mode can be excited via the grating. Both diffraction and propagation angles change with the light frequency. Therefore, in a perfectly designed grating structure, we can assume that each diffraction order can excite at least one resonance (mode) within the frequency range Δω. Therefore, the total number of resonances is the sum of resonances excited by different diffraction orders. Generally speaking, each diffraction order has different efficiency, meaning that the energy of incident light is not distributed uniformly among them. Consequently, each diffraction order has a different contribution to total absorption. For this reason, calculating the maximum absorption enhancement factor for each diffraction order is of great importance in grating design [37–39], especially for thin-film solar cells, where the absorber thickness is too small to efficiently absorb photons with energy close to the absorber band gap [40]. Among all different materials used in thin-film solar cells, (nano)-crystalline silicon (Si) is a good bench mark to study different light trapping schemes, due to its low absorption coefficient in the near infrared part of the spectrum [41].

In this paper, we apply the statistical temporal coupled-mode theoretical approach to calculate the maximum enhancement factor for each type of resonance in a grating structure. The maximum absorption enhancement for 2-D grating structure varies according to the dimensions (lattice constant) and arrangement of unit cell (hexagonal, square, triangle…). Therefore, for 2-D grating, it is not possible to write down a closed formula independent of

grating arrangement and unit cell dimensions. For this reason, in this article we only deal with one dimensional (1-D) grating structures. For our analysis, we consider normal incidence and only one polarization. Total number of resonances is then multiplied by two in order to consider two polarizations. This work is divided in two parts: first, we investigate the case of texturing at one surface. Then, we extend our calculations for double side textured structures.

2. Distinguishing the contribution of Fabry-Perot modes and wave-guided modes

Consider a periodically corrugated dielectric slab with thickness d and periodicity L, made of Si. The slab is placed on a perfect mirror and it is illuminated from above under normal incidence (Fig. 1(A)). The incident plane wave, after hitting the air-Si interface, scatters into many distinct propagating directions inside the slab.

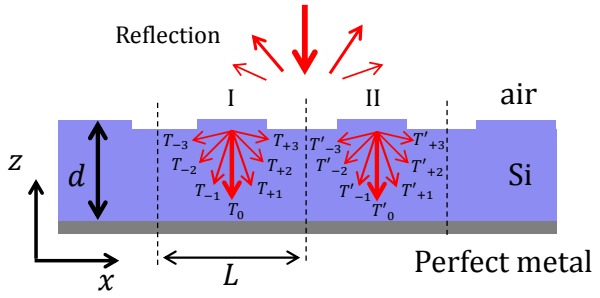

Fig. 1. Light scattering in a Si-based periodically textured structure with thickness d and period of L. The two regions, marked I and II, represent the first (T_i) and second (T'_i) scattering of the incident plane wave inside the structure, respectively. The structure is placed on a flat silver. First and second scattering both occur at Si-air interface

The scattered waves bounce along the z and x directions, exciting resonances. In such a structure, the value of the wave-number of resonances inside the film is not continuous, but is described by the following equation:

$$k_{(p,q)} = n\frac{\omega_{(p,q)}}{c} = \sqrt{\left(p\frac{2\pi}{d}\right)^2 + \left(q\frac{2\pi}{L}\right)^2} \quad \begin{cases} p = \pm 1, \pm 2, \ldots \pm \infty \\ q = 0, \pm 1, \ldots \pm \infty \end{cases} \tag{2}$$

where, ω is the angular frequency of light. Each p and q pair correspond to one resonance. The index p (q) refers to resonances excited in the z (x) direction, due to the thickness of the slab, d (period of the grating, L). Any frequency lower than $\omega_{(\pm 1,0)}$ (cut off frequency) cannot propagate inside the structure. In a frequency range $[\omega, \omega + \Delta\omega]$, the total number of resonances supported by a 1-D structure can be calculated as [42]:

$$\begin{aligned} M &= P \cdot \psi \cdot \frac{d}{d\omega}\left(\frac{\text{area of circle with radius } k = \omega \cdot n/c}{\text{area of a resonance}}\right) \cdot \Delta\omega = \ldots \\ \ldots &= P \cdot \psi \cdot 2\pi \cdot \frac{n^2\omega}{c^2}\left(\frac{L}{2\pi}\right)\left(\frac{d}{2\pi}\right)\Delta\omega \end{aligned} \tag{3}$$

where c is the speed of light *in vacuo*, P is the total number of polarizations that is taken into account ($P = 1$ for polarized light, TE or TM, $P = 2$ for non-polarized light). In this work, we only consider one polarization, therefore, $P = 1$ throughout this article. ψ is grating symmetry coefficient and has only two values, $\psi = 1$ for asymmetric and $\psi = 1/2$ for symmetric grating. In this context, an asymmetric grating is characterized by a grating whose cross-sectional period does not have mirror symmetry. According to reference [36] under normal incidence the number of resonances in symmetric grating is half of that of asymmetric grating. Because a

symmetric grating cannot couple a normal incidence, which has an even modal amplitude profile, to resonances with odd modal amplitude profile. However, if the modal amplitude of the incidence beam is not symmetric (oblique incidence), then even a symmetric grating can couple some part of the incidence energy to resonances with odd modal amplitude. In this work we are considering normal incidence, therefore, we follow the approach in [36]. Equation (3) describes the total number of resonances supported by the structure (the dots enclosed by the red circle in Fig. 2) within the frequency range [0, ω], and does not provide any information about the type of resonance. We use the same method as in Eq. (3) to count the number of resonances with different k_x. We also use k_G and k_d instead of $2\pi/L$ and $2\pi/d$, respectively, to ease the writing. In Fig. 2, a certain resonance occupies an area equal to $(q \cdot k_G) \times (p \cdot k_d)$. Each diffraction order in *k–space* occupies a minimum area of $(q \cdot k_G) \times (1 \cdot k_d)$, for example the red rectangle in Fig. 2 represents the minimum area that a second order diffraction resonance occupies $(2k_G \cdot k_d)$. Now, for a particular q^{th} (diffraction order) we can change the value of p and calculate the total area – in *k–space* – that all resonances for a particular diffraction order can occupy. Of course, any p and q pair must be chosen such that Eq. (2) still holds. For example, the grey rectangle in Fig. 2 shows total area (in the reciprocal or *k*–space) that can be possibly occupied by second diffraction order, below frequency $\omega = (k \cdot c)/n$. This area is equal to $4 \cdot q \cdot k_G \cdot k \cdot \cos(\alpha)$, where $q = 2$ (second diffraction order), $k = (n \cdot \omega)/c$, and $\theta = \arcsin(q \cdot k_G/k)$.

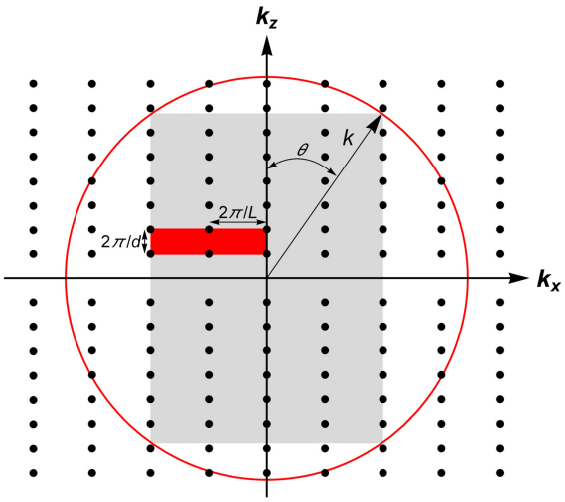

Fig. 2. Resonances (black dots) in a waveguide endowed with a 1-D grating with period L. The grey region represents the maximum area (in reciprocal *k–space*) that can be occupied by all second diffraction orders in the frequency range [0, ω]. $\theta = \arcsin(2 \cdot k_G/k)$ is the angle showing the direction of the k vector inside the material, when pointing at the highest second order resonance.

Using the same concept as Eq. (3), and using the normalized frequency $s = L / \lambda$, one can calculate the number of resonances for the q^{th} diffraction order, within the frequency range $[\omega, \omega + \Delta\omega]$:

$$M_q = 4\psi \frac{n^2 s}{c\sqrt{(ns)^2 - q^2}} \cdot \frac{d}{2\pi} \Delta\omega \qquad (4)$$

Using Eq. (4), one can count all guided resonances, but not pure Fabry-Perot (FP) resonances (i.e. those dots which are located on the k_z axis in Fig. 2, indicated with $k_{(p,0)}$). FP resonances are only defined by the optical thickness of the film and the wavelength of incident light (q =

0 in Eq. (2)). In the frequency range between $[\omega, \omega + \Delta\omega_{|\ \omega\ >\ \omega(1,0)}]$ the number of pure FP resonances can be calculated by:

$$M_{\mathrm{FP}} = \frac{d}{d\omega}\left(2\frac{k}{k_d}\right) = 2\frac{n}{k_d c}\Delta\omega \tag{5}$$

According to Eq. (2), any frequency lower than cut-off frequency cannot propagate inside the structure. Therefore, Eq. (5) is valid only for $\omega > \omega_{(1,0)}$. Now that we can count all the resonances and distinguish their origin (guided or Fabry-Perot), the total enhancement factor for each type of resonance can be calculated, using Eq. (1). If we determine M_q using Eq. (4) and then substitute the obtained value in Eq. (1), we can calculate the total enhancement factor for q^{th} diffraction order as:

$$F_q = 4\psi\frac{ns}{\sqrt{(ns)^2 - q^2}}\cdot\frac{1}{2.\psi.\lfloor s\rfloor + 1} \tag{6}$$

where $N = 2.\psi.\lfloor s\rfloor + 1$ is the number of channels (reflection orders) for this structure, and $\lfloor x\rfloor$ represents the largest integer that is smaller than x. Equation (6) shows the enhancement factor for a particular guided resonance, when $\sqrt{(L/d\cdot n)^2 + (q/n)^2} < s$. The enhancement factor for pure FP in an asymmetric grating can calculated by:

$$F_{\mathrm{FP}} = \frac{2}{2\cdot\psi\cdot\lfloor s\rfloor + 1} \tag{7}$$

The numerator indicates that a FP resonance enhances the light path 2 times. Equation (7) is only valid for $s > L/(d\cdot n)$, which is the cut-off frequency of the structure. Absorption enhancement due to FP resonance decreases as frequency increases. The symmetry of grating does not affect the total number of excited FP resonance (Eq. (5) has not dependency on ψ) but it affects absorption enhancement due to FP resonance. As an asymmetric grating could couple a FP resonance into resonances with odd or even modal amplitude profile, a FP resonance in such a grating structure has more chance to escape the system. This means that for s ≥ 1, absorption enhancement due to FP resonance is smaller in asymmetric grating than in symmetric one. For normalized frequency 0 ≤ s < 1, Eq. (7) shows identical result for symmetric and asymmetric gratings. The total (cumulative) enhancement factor is obtained by adding the enhancement factor for all diffraction orders and the pure FP resonances:

$$F_{\mathrm{TOT}} = F_{\mathrm{FP}} + \sum_{q=1}^{q=\infty} F_q \tag{8}$$

Using Eq. (8), we propose the weight of Fabry-Perot contribution to the enhancement factor (W_{FP}) as:

$$W_{FP} = \frac{F_{FP}}{F_{Total}}. \tag{9}$$

We shall use this aggregated metric in the remainder of this contribution to quantitatively distinguish the impact of Fabry-Perot resonances on total absorption enhancement factor.

3. Extending the temporal couple-mode theory to different thicknesses

According to Eq. (2), the wavenumber must reach the minimum value $k_{\min} = \sqrt{(2\pi/d)^2 + (q2\pi/L)^2}$, in order to excite the lowest mode (p = 1) of the q^{th} diffraction

Optics EXPRESS

order. Therefore, the normalized frequency must be $s > \sqrt{\left(L/(n\cdot d)\right)^2 + \left(q/n\right)^2}$ to excite the first guided resonance of the q^{th} diffraction order. Here the thickness of the film comes into account. In fact, the larger the optical thickness ($n \cdot d$) of the film is with respect to the grating period ($L/(n\cdot d) \to 0$), the closer the system behaves like in the bulk regime, and vice versa. Thus, only in the range $\sqrt{\left(L/(n\cdot d)\right)^2 + \left(q/n\right)^2} < s$ Eq. (4) counts the guided modes. This clearly shows that the slab thickness has an impact on the maximum absorption enhancement. For example, Eq. (6) indicates that if $s \to q/n$, then $F_q \to \infty$. However, the condition $s > \sqrt{\left(L/(n\cdot d)\right)^2 + \left(q/n\right)^2}$ must be respected. Therefore, only for a film with very large optical thickness ($L/(n\cdot d) \to 0$) the enhancement factor can be infinitely large. As an extreme example, the result of Eqs. (6) to (8) for an *overly* thick slab with d = 1 mm (Fig. 3(A)) is presented in Fig. 3(B). The black curve represents the cumulative absorption enhancement in a film with the physical thickness of 1 mm ($L/(n\cdot d) = 1.5\times10^{-4}$) with n = 4, endowed with 1-D asymmetric texturing. At $s = q / n$, a new diffraction order appears. Therefore, a peak in the guided mode enhancement (grey curve) and in the total enhancement (black curve) is observed. Since the diffraction angle decrease as frequency increases, the enhancement drops dramatically until $s = (q + 1) / n$, where a new peak appears. At s = 1, the number of channels (reflection orders) increases from 1 to 3 and therefore the enhancement drops suddenly. In Fig. 3(C) we present W_{FP} related to the structure shown in Fig. 3(A). For s < 0.25 (considering $s = q / n$, with n = 4 and q = 1), no diffraction order exists and all the absorption enhancement is due to FP resonance, therefore, $F_{TOT} = F_{FP}$ and W_{FP} = 100%. At s = 0.25 the first diffraction order arises. The absorption is significantly enhanced due to presence of such first diffraction order (see the black curve at s = 0.25 in Fig. 3(B)), whereas F_{FP} does not change (see the blue curve in Fig. 3(B), for $0 < s < 1$, F_{FP} does not vary). As $F_{TOT} = F_{FP} + F_{q=\pm1}$, where $F_{q=\pm1} >> F_{FP}$, W_{FP} drops suddenly. $F_{q=\pm1}$ decreases as the normalized frequency increases and, therefore, W_{FP} grows rapidly until reaches its maximum (around 30%) at $s \to 0.5$. For s = 0.5 another diffraction order arises and thus W_{FP} drops again. This sequence repeats: for s approaching q / n, W_{FP} is peaks and for $s = q / n$ the W_{FP} is minimum.

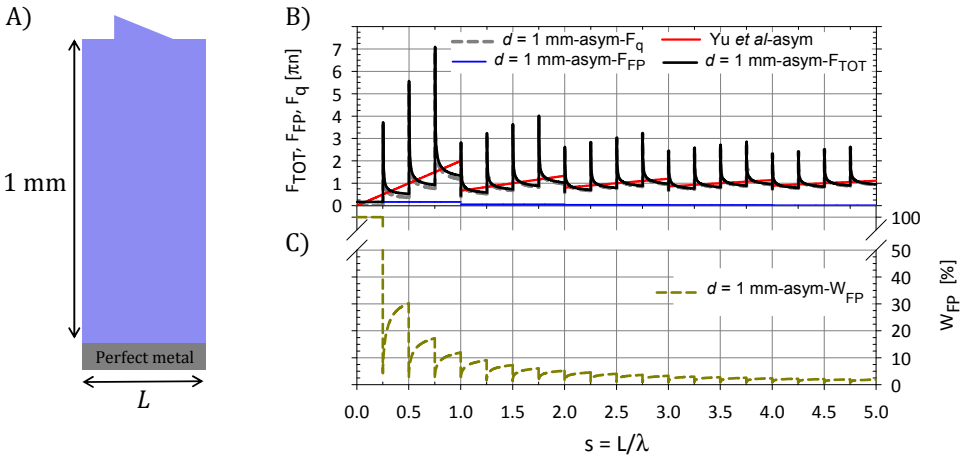

Fig. 3. (A) Schematic presentation of an *overly* thick structure with asymmetric grating. (B) Absorption enhancement achievable in a thick Si film with 1-D asymmetric periodic texturing (d = 1 mm). The maximum enhancement achieved by the guided and FP resonances are shown by dashed grey and solid blue lines, respectively. Their sum results in the total enhancement (black line). The red curve represents the maximum enhancement factor calculated by Yu *et al.* (C) represents the W_{FP} for the structure shown in (A).

Optics EXPRESS

So far, only asymmetric grating has been considered. The number of channels are also influenced by the symmetry of the grating and becomes $N_{sym} = \lfloor s \rfloor + 1$. Therefore, the maximum enhancement achieved by symmetric grating would be half of asymmetric one. The graph in Fig. 4(B) shows the absorption enhancement in a symmetric grating structure with the unrealistic thickness of 1 mm (identical thickness to the structure in Fig. 3(A)). One can clearly see that the maximum absorption enhancement is half of the one for asymmetric grating (Fig. 3(B)). Thus, for a film with $d \to \infty$, we observe that (a) the maximum theoretical enhancement tends to infinite for both symmetric and asymmetric gratings and (b) the symmetry of the grating profile does not play any role in defining maximum absorption enhancement. In Fig. 4(C) the W_{FP} related to the structure shown in Fig. 4(A) is presented. Comparing Fig. 4(C) and Fig. 3(C), one can observe that in a structure with symmetric grating (Fig. 4(A)) the W_{FP} is larger than in a structure with asymmetric grating (Fig. 3(A)). This is due to the fact that a structure with symmetric grating has smaller F_{TOT} than a structure with asymmetric grating, while both structures have the same F_{FP}. Therefore, W_{FP} is larger in structure endowed with symmetric grating.

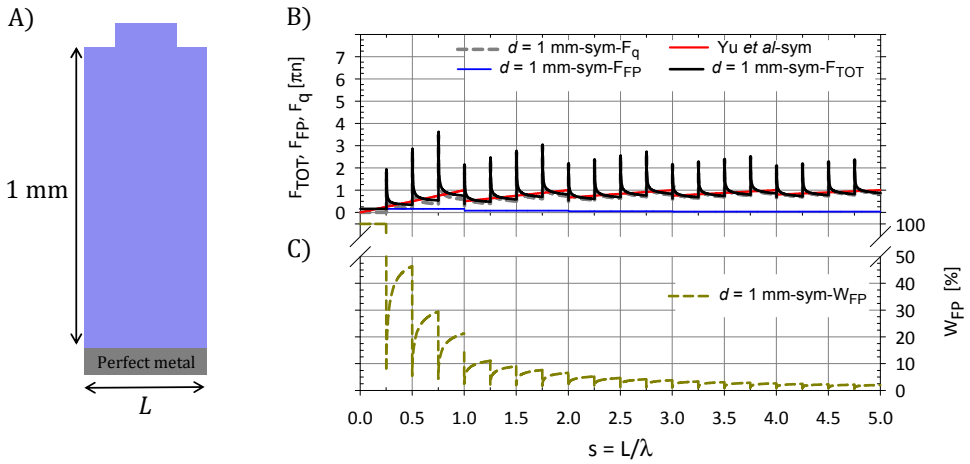

Fig. 4. (A) Schematic presentation of a thick structure with a symmetric grating. (B) Absorption enhancement in a thick Si slab with thickness-to-period ratio $L/(n \cdot d) = 1.5 \times 10^{-4}$ ($d = 1\,\text{mm}$) endowed with a symmetric grating. (C) represents the W_{FP} for the structure shown in (A).

3.1 Maximum enhancement frequency in bulk regime

The maximum enhancement frequency for bulk structures (i.e. the frequency at which the enhancement is maximum) occurs when the denominator in Eq. (6) tends to zero, i.e. $s \to q/n$. On the other hand, for $s \geq 1$ the number of channels increases, which results in a drop of enhancement. From these two conditions, we can conclude that s_{max} can be calculated using equation below:

$$s_{max} = \lim_{q \to n^-} \frac{q}{n} \tag{10}$$

The refractive index n can be any positive real number, whereas q can only be an integer. Therefore, depending on whether n is an integer or not we get two cases: (i) if n is an integer the maximum frequency occurs for $q = n - 1$; (ii) if n is not an integer, s_{max} occurs for $q = \lfloor n \rfloor$. In this work, since we assume $n = 4$ for both symmetric and asymmetric structures, the maximum enhancement occurs at $s = 0.75$, where the third diffraction order has the largest propagation angle and there is only one channel (reflection order).

Optics EXPRESS

3.2 Maximum enhancement in thin film regime

So far, we have discussed the case of a film with a very large thickness. As mentioned earlier, when L/d increases, the lowest frequency to excite the first resonance for a diffraction order is increased. Therefore, the peaks in Eq. (6) do not occur at $s = q/n$, but rather at $s = \sqrt{\left(L/(n \cdot d)\right)^2 + (q/n)^2}$. This situation is illustrated in Fig. 5(B) where the absorption enhancement for an asymmetric grating structure with thickness of 1 μm is shown (Fig. 5(A)). The maximum absorption enhancement occurs at around $s = 0.76$ rather than 0.75. Additionally, since the structure is thin, its cut off frequency occurs at higher frequency. This can be observed in Fig. 5(B) where $F_{FP} \neq 0$ for $s \geq 0.15$ rather than $s = 0$. Although, changing the thickness influences the cut-off frequency, it does not affect the W_{FP} much. In Fig. 5(C) the W_{FP} is only slightly shifted to the right with respect to Fig. 3(C), but its maximum and minimum values remains unchanged.

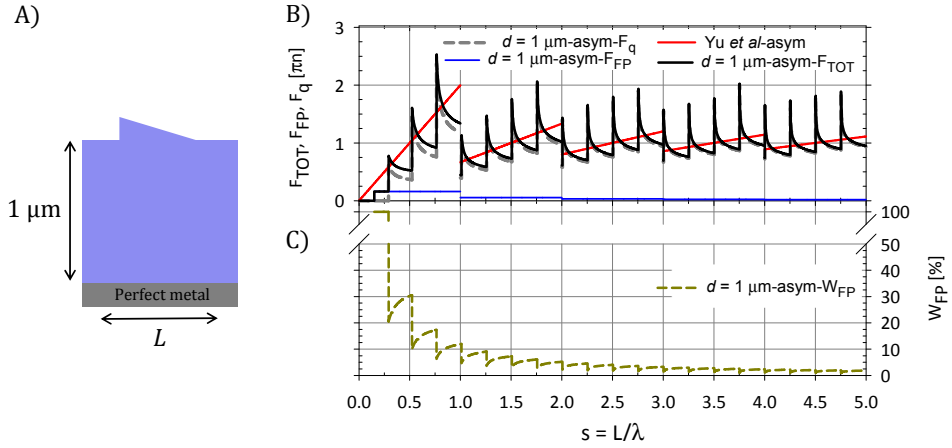

Fig. 5. (A) Schematic presentation of a 1000-nm thick Si film endowed with asymmetric grating. (B) Shows the absorption enhancement in the structure shown in (A). Dashed grey and solid blue lines represent the enhancement due to guided and FP resonances, respectively, while the solid black curve is their sum. The red line is the limit calculated by Yu *et al*. for an asymmetric grating structure. (C) represents the W_{FP} for the structure shown in (A).

The absorption enhancement is lower for a thin film with a symmetric grating. The graph in Fig. 6(B) presents the absorption enhancement achieved in a 1000-nm thick film with a symmetrical grating (Fig. 6(A)). Although symmetric gratings have much lower maxima than asymmetric gratings, it still higher than what is predicted by Yu *et al.*, but for a small frequency range. The graph in Fig. 6(C) illustrates the W_{FP} related to the structure shown in Fig. 6(A). As it has been elaborated earlier, changing the thickness does not influence the maximum or minimum values for W_{FP}, but the W_{FP} is shifted to left or right for decreasing of increasing the thickness, respectively.

Optics EXPRESS

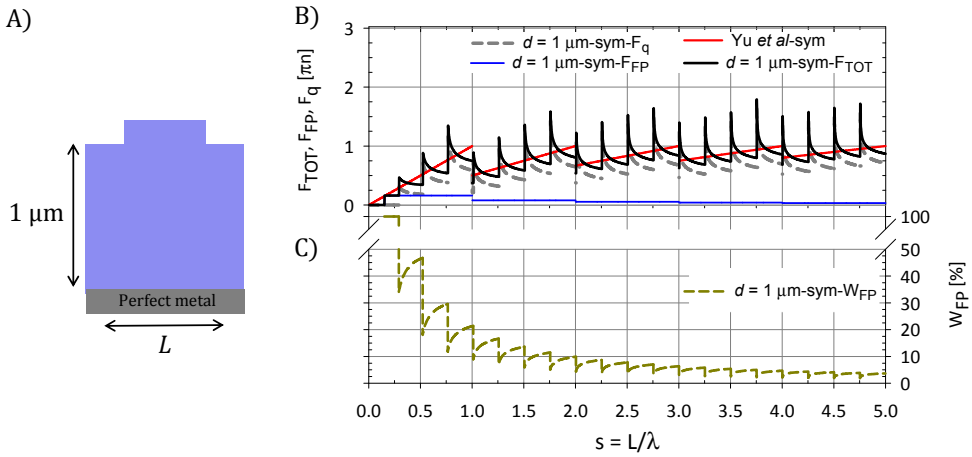

Fig. 6. (A) Schematic presentation of a 1000-nm thick Si film endowed with symmetric grating. (B) Shows the absorption enhancement in the structure shown in (A). Dashed grey and solid blue lines represent the enhancement due to guided and FP resonances, respectively, while the solid black curve is their sum. The red line is the limit calculated by Yu *et al*. for a symmetric grating structure. (C) represents the W_{FP} for the structure shown in (A).

To test our theoretical analysis, we rigorously calculate the absorption enhancement using a symmetric and an asymmetric grating structure shown in Fig. 7(A) and Fig. 8(A) respectively. Both gratings have a duty cycle of 50%, height h = 20 nm and period of L = 600 nm. The structures have a thickness of d = 1000 nm. We use TE polarized light under normal incidence within the wavelength range [750 nm, 1100 nm] ($0.54 < s < 0.8$). We use COMSOL Multiphysics, a finite element analysis (FEA) solver, as a modelling tool to rigorously calculate the electromagnetic field inside the absorber. Periodic boundary condition is used to calculate the electric field in the periodic structure. The electric field is then decomposed into its spatial components, using Fourier expansion to calculate the absorption enhancement for each diffraction order [43]. Since Si is a dispersive material, in this simulation we use wavelength-dependent $n(\lambda)$ and $k(\lambda)$ data of nc-Si:H [44]. The wavelength-dependent absorption coefficient, α, can be calculated using $k(\lambda)$ via $\alpha(\lambda) = 4\pi k(\lambda)/\lambda$. The wavelength-dependency of α implies that γ_i is also a function of wavelength. The electric field inside the structure is calculated for each wavelength, using the wavelength-dependent n and k data. The result for symmetric grating is illustrated in Fig. 7(B). Each color represents the absorption enhancement for one diffraction order. There are peaks well beyond both the asymmetric and symmetric 1-D nano-photonic limit ($2\pi n$ and πn, respectively), and one even exceeding the 2-D Lambertian bulk limit ($4n^2$). This example shows that for a limited frequency range, the enhancement can significantly exceed the nano-photonic limit. Comparing Fig. 6(B) and Fig. 7(B) one can realize that the absorption enhancement is larger than what is predicted by our theoretical model. One of the reasons is that the analytical approach does not consider the multiple scattering in the structure. It counts each resonance only for the first scattering event (T_i). Whereas, in the rigorous calculation, multiple scattering events are taken into account (T_i and T_i'). Therefore, the simulation shows a higher absorption enhancement.

Optics EXPRESS

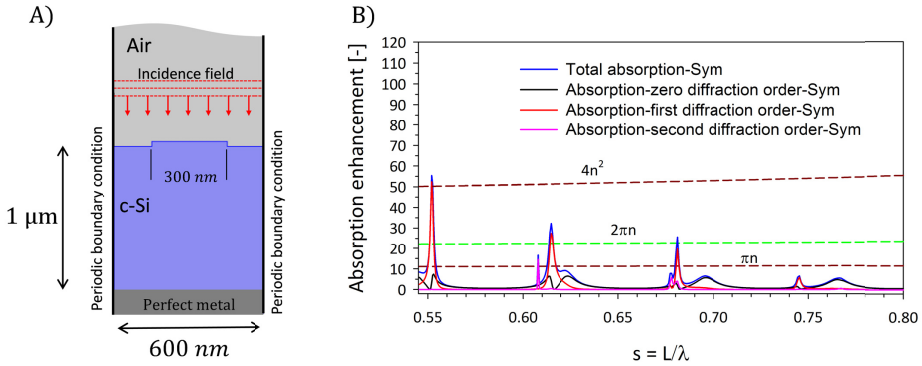

Fig. 7. (A) shows one period of a 1 μm thick Si slab endowed with a symmetric grating. The grating has a period of 600 nm, duty cycle 50% and height of 20 nm. The structure is excited using normal incidence plane wave. The electric field inside the Si slab is calculated using COMSOL multyphysics. (B) Shows the absorption enhancement in the structure shown in (A), total absorption at each wavelength is divided by the one pass absorption [43] at corresponding wavelength, to calculate the enhancement. Absorption enhancement for each grating order is also presented in different color.

In Fig. 8(A), one period of a 1-μm thick Si slab endowed with an asymmetric grating is shown. The only difference between Fig. 7(A) and Fig. 8(A) is the symmetry of the grating; other specifications are identical. In Fig. 8-B one can see the absorption enhancement for each diffraction order for the structure shown in Fig. 8(A). Here, similar to Fig. 7(B), the peaks exhibit values well beyond both the asymmetric and symmetric 1-D nano-photonic limit ($2\pi n$ and πn, respectively), and the 2-D Lambertian bulk limit ($4n^2$). The absorption enhancement at s = 0.55 and 0.62 are almost double in Fig. 8-B with respect to Fig. 7(B).

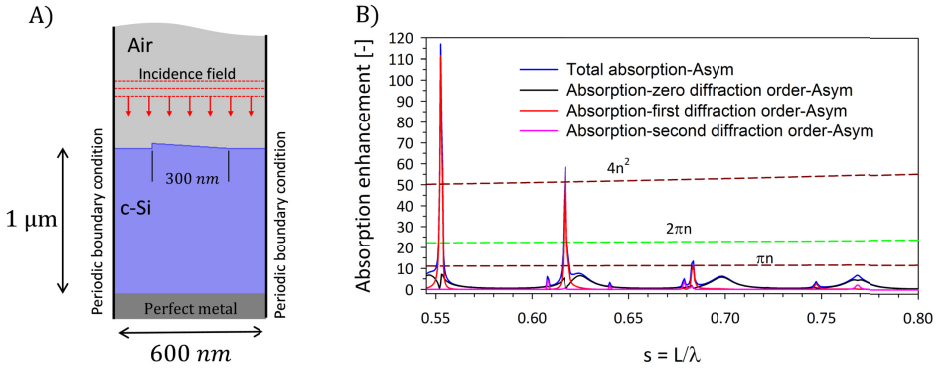

Fig. 8. (A) shows one period of a 1-μm thick Si slab endowed with an asymmetric grating. The grating has a period of 600 nm, duty cycle 50% and height of 20 nm. The structure is excited using normal incidence plane wave. The electric field inside the Si slab is calculated using COMSOL multyphysics. (B) Shows the absorption enhancement in the structure shown in (A), total absorption at each wavelength is divided by the one pass absorption [43] at corresponding wavelength, to calculate the enhancement. Absorption enhancement for each grating order is also presented in different color.

4. Absorption enhancement in double side textured slab

So far, we discussed the case of a single grating structure on a flat mirror. In real thin film solar cells, however, both interfaces might be corrugated, due to manufacturing processes. Now, let us consider a Si slab with thickness of *d,* having each interface textured with a different periodicity, L_{top} and L_{bot} respectively. In Fig. 9 light scattering from top (T_i) and bottom (T'_i) interfaces of a double side textured slab is shown. Texturing the second interface

with different periodicity allows the light to be re-scattered with different angular distribution, thus exciting more resonances. The scale of the structure in Fig. 9 is only for presentation purposes and it is not related to our calculation. Attempting to find the maximum absorption enhancement achievable in such an optical system entails to extend the temporal coupled-mode theory as put forward by Yu et al. [35,36], since it handles only one side texturing.

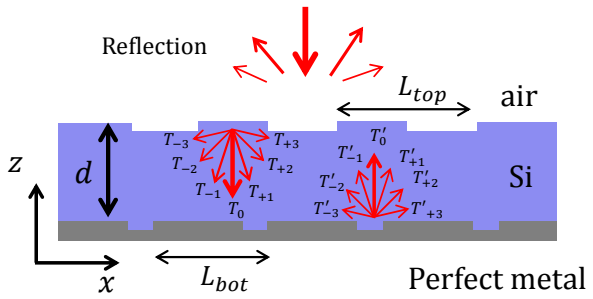

Fig. 9. Light scattering in a double side periodically textured Si-based slab. The periods of top and bottom gratings are indicated as L_{top} and L_{bot} respectively. The structure has a thickness d. The first and second scattering of the incident plane wave inside the structure, is indicated by T_i and T'_1 respectively. The structure is placed on a grating made of a perfectly reflecting metal. Here, second scattering occurs at the Si-metal interface.

Therefore, we suggest that the total number of resonances M_{double} is the sum of resonances excited by the top (M_t) and bottom gratings (M_b). The total number of resonances in a 1-D structure with double side periodic texturing in the frequency range [ω, ω + Δω] can be thus calculated as:

$$M_{double} = 2\pi \frac{n^2 \omega}{c^2}\left(\psi_{top}\frac{L_{top}}{2\pi} + \psi_{bot}\frac{L_{bot}}{2\pi}\right)\left(\frac{d}{2\pi}\right)\Delta\omega \tag{11}$$

where L_{top} and L_{bot} are the periodicity of the top and bottom interfaces, respectively . ψ_{top} and ψ_{bot} are the symmetry coefficient for top and bottom gratings respectively. To count the number of resonances based on the diffraction order, we need to use Eq. (4) for top and bottom grating separately. Doing so, we arrive at:

$$M_{t,b} = 4\frac{n^2}{c}\cdot\frac{d}{2\pi}\left(\psi_{top}\frac{s_t}{\sqrt{(ns_t)^2 - q_t^2}} + \psi_{bot}\frac{s_b}{\sqrt{(ns_b)^2 - q_b^2}}\right)\Delta\omega \tag{12}$$

where $s_t = L_{top}/\lambda$ and $s_b = L_{bot}/\lambda$ are the normalized frequency of the top and bottom interfaces, respectively; and q_t and q_b are the q^{th} diffraction order of the top and bottom gratings, respectively. If the solar cell is placed on a mirror, then the number of leakage channels (N) only depends on the periodicity of the top interface. If the mirror is not present, N is the sum of channels from top and bottom interfaces. Combining Eqs. (1) and (12), we can obtain the enhancement factor per diffraction order:

$$F_{t,b} = \frac{4n}{2\psi_{top}\lfloor s_t \rfloor + 1}\left(\psi_{top}\frac{s_t}{\sqrt{(ns_t)^2 - q_t^2}} + \psi_{bot}\frac{s_b}{\sqrt{(ns_b)^2 - q_b^2}}\right) \tag{13}$$

This equation is a linear sum of the enhancement achieved by the top and bottom surfaces. If we plot the enhancement from top or bottom gratings individually, a graph very similar to Fig. 3 or Fig. 4 can be obtained, depending on the symmetry of the grating. Note that for double side texturing top and bottom gratings could have different symmetry. However, since normalized frequency is directly linked to the grating period, the plot for the bottom grating

Optics EXPRESS

might be shifted to the right or left with respect to the plot for the top grating. The amount of shift depends on the ratio between L_{top} and L_{bot}. If $L_{top}/L_{bot} > 1$, there is a shift toward high frequencies. On the other hand, for $L_{top}/L_{bot} < 1$, a shift toward low frequencies occurs. For $L_{top}/L_{bot} = 1$, no shift is observed. The L_{top}/L_{bot} ratio can be defined according to the applications. In thin film solar cell, it is desirable to increase the absorption in a wide range of frequencies close to the band gap of the material. Therefore, the L_{top}/L_{bot} ratio should be smaller than one. L_{top} should be smaller than the band gap wavelength. On the other hand, L_{bot} should be larger than L_{top}, to ensure maximum excitation of modes. Figure 10(A) schematically shows a slab with double side texturing, the top and bottom gratings are symmetric but they have different periods. The structure in Fig. 10(A) is only used for presentation purposes; the scale of top and bottom grating is exaggerated and it is not used for our calculation. In Fig. 10(B) one can see the cumulative enhancement factor calculated for a double side textured film with a thickness of 1000 nm. The period of top and bottom symmetric gratings are 600 nm and 660 nm respectively. Since $L_{top}/L_{bot} < 1$ the red curve is shifted to the left with respect to the blue curve. As it can be seen in Fig. 10-B, the solid black line has more peaks than either blue or red curves.

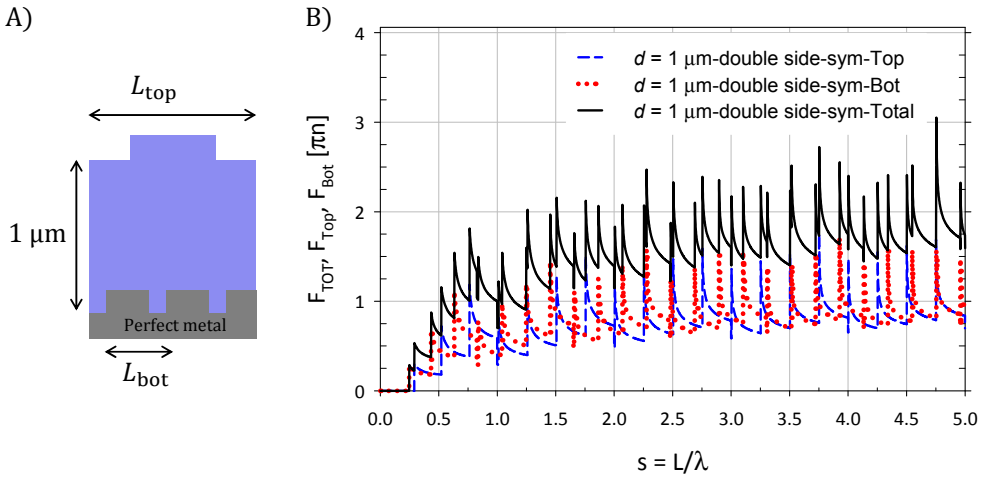

Fig. 10. (A) schematically shows a 1-µm thick slab endowed with symmetric grating on two interfaces. The scale of top and bottom grating is exaggerated only for purpose of visualization; (B) reports the absorption enhancement from top (blue) and bottom (red) symmetric gratings in a 1000-nm thick Si film. The ration for L_{top} / L_{bot} is equal to 0.909. Total enhancement is shown in black line.

The structure in Fig. 11(A) shows a 1-µm thick slab endowed with asymmetric grating on top and bottom interfaces. The top and bottom gratings have different periods, the scale of top and bottom grating is exaggerated and it is not used for our calculation.

Figure 11(B) represents the absorption enhancement in a structure with double side texturing with asymmetric grating. Apart from the grating symmetry, the structure is identical to the one we used for Fig. 10(A).

Optics EXPRESS

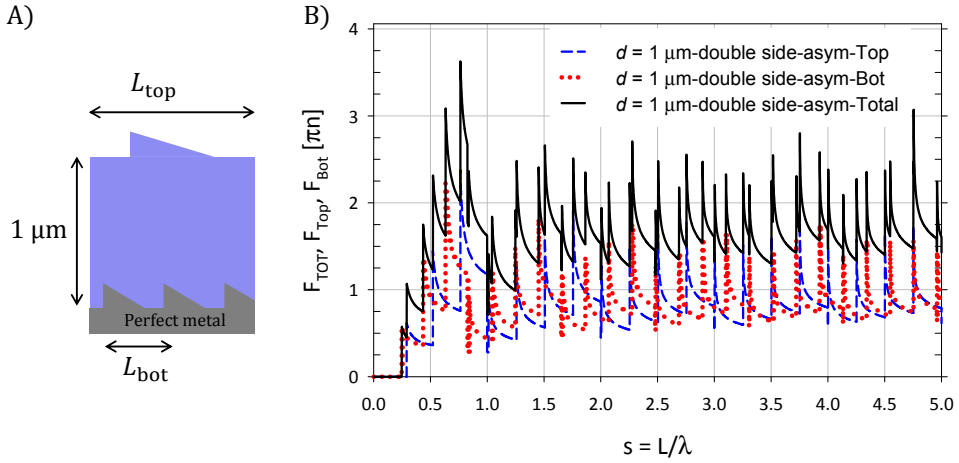

Fig. 11. (A) Schematically shows a 1-μm thick slab endowed with asymmetric grating on two interfaces. The scale of top and bottom grating is exaggerated only for purpose of visualization; (B) reports the absorption enhancement from top (blue) and bottom (red) asymmetric gratings in a 1000-nm thick Si film. The ration for L_{top} / L_{bot} is equal to 0.909. Total enhancement is shown in black line.

In conformal texturing (L_{top}/L_{bot} = 1), peaks resulting from the excitation of modes by top and bottom grating overlap, creating larger peaks ($F_{t,,b} = 2F_q$). However, the absorption is not enhanced spectrally. In solar cell application, it is desirable to design top and bottom gratings such that none of the peaks from top and bottom gratings overlap. Therefore, L_{top} should be an aliquant part of L_{bot}, or vice versa [45,46]. In this way, no multiple of the top grating vector ($q_{top} \cdot k_{top}$) is equal to a multiple of the bottom grating vector ($q_{bot} \cdot k_{bot}$). In other words, none of the diffraction angles from top surface matches with bottom diffraction angles.

5. Conclusions

Leveraging the temporal coupled-mode theory, we have used an alternative method to calculate total number of resonances with same $|k_x|$ in the frequency range [ω, ω + Δω] supported by a grating structure. Our results allow for calculating the maximum absorption enhancement for each diffraction order in 1-D grating structure. We discussed the influence of grating symmetry as well as the film thickness in absorption enhancement. We have shown that in a 1-D grating structure, the absorption can be enhanced much more than 2πn in multiple frequencies (Fig. 7). The maxima in cumulative absorption enhancement depends on the grating period, slab thickness and absorber refractive index (see Eq. (6)). For n = 4, the absolute maximum occurs when the third diffraction order is active. Furthermore, we have also shown that weight of Fabry-Perot resonances on the total enhancement factor can be computed. In all treated cases, such weight stays below 50% for symmetric and below 30% for asymmetric grating. Moreover, it has been shown that weight of Fabry-Perot resonances on the total enhancement factor does not change with the thickness of the slab. We have also shown that for achieving even higher absorption enhancement within a larger frequency range a double-side grating-textured absorption slab should be considered, in which L_{top} should be an aliquant of L_{bot}, or vice versa (see Eq. (13)). This last result further extends the temporal coupled-mode theory as proposed by Yu et al.

Finally, we did not consider 2-D gratings in this work, because it is not possible to derive a closed formula independent of grating arrangement and unit cell dimensions. Nevertheless, we expect similar trends in 2-D case. Meaning that, in higher normalized-frequency, the value for absorption enhancement in 2-D structure, would reach the 2-D bulk limit of $4n^2$, but for low frequencies we expect higher absorption enhancement.

Optics EXPRESS

References

1. A. Reinders, P. Verlinden, W. Sark, and A. Freundlich, *Photovoltaic Solar Energy: From Fundamentals to Applications*, (John Wiley & Sons, Ltd, 2017).
2. M. Zeman, O. Isabella, S. Solntsev, K. Jäger, "Modelling of thin-film silicon solar cells," Solar Energy Materials and Solar Cells **119** (2013).
3. L. C. Andreani, A. Bozzola, P. Kowalczewski, M. Liscidini & L. Redorici,"Silicon solar cells: toward the efficiency limits," Advances in Physics: X, **4**(1), 1548305 (2019).
4. T. Matsui, H. Jia, M. Kondo, K. Mizuno, S. Tsuruga, S. Sakai, and Y. Takeuchi, "Application of microcrystalline Si1xGex infrared absorbers in triple junction solar cells, in: 35th IEEE Photovoltaic Specialists Conference (PVSC), 2010, 311–316.
5. H. M. Lee, S. W. Ahn, S. E. Lee, and J. H. Choi, Silicon thin film technology applications for low cost and high efficiency photovoltaics, in: Technical Digest of the21st International Photovoltaic Science and Engineering Conference (PVSEC-21), 4A–2I-01, Fukuoka, Japan, 2011.
6. B. Yan, G. Yue, L. Sivec, J. Yang, S. Guha, and C.-S. Jiang, "Innovative dual function nc-SiOx:H layer leading to a >16% efficient multi-junction thin-film silicon solar cell," Appl. Phys. Lett. **99**(11), 113512 (2011).
7. K. Söderström, G. Bugnon, R. Biron, C. Pahud, F. Meillaud, F.-J. Haug, and C. Ballif, "Thin-film silicon triple-junction solar cell with12.5% stable efficiency on innovative flat light-scattering substrate," J. Appl. Phys. **112**(11), 114503 (2012).
8. H. Sakaki, T. Tanoue, K. Yokoyama, D. C. Sun, Y. Sekiguchi, and Y. Yukimoto, "Design and performances of a triple (GaAs, Si, and Ge)-solar-cell system with multi-layered spectrum splitters," Jpn. J. Appl. Phys. **20**(S2), 127–133 (1981).
9. A. Barnett, D. Kirkpatrick, C. Honsberg, D. Moore, M. Wanlass, K. Emery, R. Schwartz, D. Carlson, S. Bowden, D. Aiken, A. Gray, S. Kurtz, L. Kazmerski, M. Steiner, J. Gray, T. Davenport, R. Buelow, L. Takacs, N. Shatz, J. Bortz, O. Jani, K. Goossen, F. Kiamilev, A. Doolittle, I. Ferguson, B. Unger, G. Schmidt, E. Christensen, and D. Salzman, "Very high efficiency solar cell modules," Prog. Photovolt. Res. Appl. **17**(1), 75–83 (2009).
10. K. Sinae, F. Takahashi, S. Kasashima, P. Sichanugrist, T. Kobayashi, T. Nakada, and M. Konagai, Development of thin-film solar cells using solar spectrum splitting technique, in: 38th IEEE Photovoltaic Specialists Conference (PVSC), 1209–1211 (2012).
11. C. Das, A. Lambertz, J. Hüpkes, W. Reetz, and F. Finger, "A constructive combination of antireflection and intermediate-reflector layers for a-Si/μc-Si thin film solar cells," Appl. Phys. Lett. **92**(5), 053509 (2008).
12. D. Dominé, P. Buehlmann, J. Bailat, A. Billet, A. Feltrin, and C. Ballif, "Optical management in high-efficiency thin-film silicon micromorph solar cells with a silicon oxide based intermediate reflector," Phys. Status Solidi Rapid Res. Lett. **2**(4), 163–165 (2008).
13. S. Faÿ, J. Steinhauser, S. Nicolay, and C. Ballif, "Polycrystalline ZnO:B grown by LPCVD as TCO for thin film silicon solar cells," Thin Solid Films **518**(11), 2961–2966 (2010).
14. T. Koida, H. Fujiwara, and M. Kondo, "Reduction of optical loss in hydrogenated amorphous silicon/crystalline silicon heterojunction solar cells by high- mobility hydrogen-doped In2O3 transparent conductive oxide," Appl. Phys. Express **1**, 041501 (2008).
15. A. Soteris, Kalogirou, McEvoy's, *Handbook of Photovoltaics,* 439–472 (Academic University, 2018).
16. V. Steenhoff, M. Juilfs, R. E. Ravekes, M. Vehse, and C. Agert, "Resonant-cavity-enhanced a-Ge:H nanoabsorber solar cells for application in multijunction devices," Nano Energy **27**, 658–663 (2016).
17. P. Yeh and N. Yeh, "Dsign and analysis of solar-tracking 2D Fresnel lens-based two staged, spectrum-splitting solar concentrators," Renew. Energy **120**, 1–13 (2018).
18. A. Dorodnyy, V. Shklover, L. Braginsky, C. Hafner, and J. Leuthold, "High-efficiency spectrum splitting for solar photovoltaics," Sol. Energy Mater. Sol. Cells **136**, 120–126 (2015).
19. M. A. Green, SolarCells: *Operating Principles, Technology, and System Applications*, (Prentice Hall, 1981).
20. J. Krč, F. Smole, and M. Topič, "Advanced optical design of tandem micromorph silicon solar cells," J. Non-Cryst. Solids **352**(9-20), 1892–1895 (2006).
21. T. Fujibayashi, T. Matsui, and M. Kondo, "Improvement in quantum efficiency of thin film Si solar cells due to the suppression of optical reflectance at transparent conducting oxide/Si interface by TiO2/ZnO antireflection coating," Appl. Phys. Lett. **88**(18), 183508 (2006).
22. S. A. Boden and D. M. Bagnall, "Optimization of moth-eye antireflection schemes for silicon solar cells," Prog. Photovolt. Res. Appl. **18**(3), 195–203 (2010).
23. M. Y. Chiu, C. H. Chang, M. A. Tsai, F. Y. Chang, and P. Yu, "Improved optical transmission and current matching of a triple-junction solar cell utilizing sub-wavelength structures," Opt. Express **18**(S3 Suppl 3), A308–A313 (2010).
24. J. Escarré, K. Söderström, M. Despeisse, S. Nicolay, C. Battaglia, G. Bugnon, L. Ding, F. Meillaud, F.-J. Haug, and C. Ballif, "Geometric light trapping for high efficiency thin film silicon solarcells," Sol. Energy Mater. Sol. Cells **98**, 185–190 (2012).
25. B. Ralf, Wehrspohn, A. G., Uwe Rau, Ed. *Photon Management in Solar Cells*, pp 120, (Wiley-VCH Verlag GmbH Co. KGaA, 2015).

Optics EXPRESS

26. C. Battaglia, C. M. Hsu, K. Söderström, J. Escarré, F. J. Haug, M. Charrière, M. Boccard, M. Despeisse, D. T. Alexander, M. Cantoni, Y. Cui, and C. Ballif, "Light trapping in solar cells: can periodic beat random?" ACS Nano **6**(3), 2790–2797 (2012).
27. H. W. Deckman, C. R. Wronski, H. Witzke, and E. Yablonovitch, "Optically enhanced amorphous silicon solar cells," Appl. Phys. Lett. **42**(11), 968–970 (1983).
28. H. Deckman, J. Dunsmuir, and J. Vac, "Applications of surface textures produced with natural lithography," Sci. Technol., B: Microelectron. Nanometer Struct. – Process., Meas," Phenom **1**, 1109–1112 (1983).
29. S. C. Stefano, *Diffractive optics for thin-film silicon solar cells*. (Springer, 2016).
30. E. Yablonovitch, "Statistical ray optics," Journal of the Optical Society of America **72**, 899–907, (1982).
31. J. H. Lambert, *Photometria, sive de mensura et gradibus luminis, colorum et umbrae* (W.Engelmann, Leipzig, 1892)
32. P.Campbell, M. A. Green, "Light trapping properties of pyramidally textured surfaces," Journal of Applied Physics **62**, 243–249, (1987).
33. E. Yablonovitch, G. D. Cody, "Intensity enhancement in textured optical sheets for solar cells," IEEE Transactions on Electron Devices **29**, 300–305, (1982).
34. Eugene Hecht, *Optics* (Addison-Wesley, 1998)
35. Z. Yu, A. Raman, and S. Fan, "Fundamental limit of nanophotonic light trapping in solar cells," Proceedings of the National Academy of Sciences of the United States of America **107**, 17491 6 (2010).
36. Z. Yu, A. Raman, and S. Fan, "Fundamental limit of light trapping in grating structures," Opt. Express **18**(Suppl 3), A366–A380 (2010).
37. A. Naqavi, F. J. Haug, C. Ballif, T. Scharf, and H. P. Herzig, "Limit of light coupling strength in solar cells," Appl. Phys. Lett. **102**(13), 131113 (2013).
38. F.-J. Haug, K. Söderström, A. Naqavi, and C. Ballif, "Resonances and absorption enhancement in thin film silicon solar cells with periodic interface texture," J. Appl. Phys. **109**(8), 084516 (2011).
39. H. R. Stuart and D. G. Hall, "Thermodynamic limit to light trapping in thin planar structures," J. Opt. Soc. Am. A **14**(11), 3001–3008 (1997).
40. C. Schinke, P. C. Peest, J. Schmidt, R. Brendel, K. Bothe, M. R. Vogt, I. Kröger, S. Winter, A. Schirmacher, S. Lim, H. T. Nguyen, and D. MacDonald, "Uncertainty analysis for the coefficient of band-to-band absorption of crystalline silicon," AIP Adv. **5**(6), 067168 (2015).
41. F. J. Haug and C. Ballif, "Light management in thin film silicon solar cells," Energy Environ. Sci. **8**(3), 824–837 (2015).
42. Charles Kittel, *Introduction to Solid State Physics*, seventh edition, (Wiley, New York, 1995).
43. H. Ahmadpanahi, R. Vismara, O. Isabella, and M. Zeman, "Distinguishing Fabry-Perot from guided resonances in thin periodically-textured silicon absorbers," Opt. Express **26**(18), A737–A749 (2018).
44. M. A. Green and M. J. Keevers, "Optical properties of intrinsic silicon at 300 K," Prog. Photovolt. Res. Appl. **3**(3), 189–192 (1995).
45. O. Isabella, R. Vismara, D. N. P. Linssen, K. X. Wang, S. Fan, and M. Zeman, "Advanced light trapping scheme in decoupled front and rear textured thin-film silicon solar cells," Sol. Energy **162**, 344–356 (2018).
46. W. C. Hsu, J. K. Tong, M. S. Branham, Y. Huang, S. Yerci, S. V. Boriskina, and G. Chen, "Mismatched front and back gratings for optimum light trapping in ultra-thin crystalline silicon solar cells," Opt. Commun. **377**, 52–58 (2016).